Solid State Sciences 152 (2024) 107524

Contents lists available at ScienceDirect

Solid State Sciences

journal homepage: www.elsevier.com/locate/ssscie

Phase change memory materials: Why are alloys of Ge, Sb, and Te the materials of choice?

Robert O. Jones [1]

Forschungszentrum Jülich, Peter Grünberg Institut PGI-1 and JARA-HPC, Jülich, 52425, Germany

ARTICLE INFO

Keywords:
Phase change memory
Alloys of Ge/Sb/Te

ABSTRACT

Rewritable optical storage is dominated by alloys of a small number of elements, particularly Ge, Sb, and Te, and Ge/Sb/Te alloys in the composition range $(GeTe)_{1-x}(Sb_2Te_3)_x$ ($0 \leq x \leq 1$) have been the materials of choice: all have metastable rock salt structures that change little over decades at archival temperatures, and all contain vacancies (cavities). The special status arises from the close similarity of the valence orbitals of Ge, Sb, and Te, which arises from the irregular changes in atomic orbitals and properties as the atomic number increases ("secondary periodicity"). The instability of cubic (metallic) Bi to a (semimetallic) rhombohedral structure (H. Jones, 1934) can be adapted to Ge/Sb/Te alloys and explains the crucial metastable (rock salt) structures of these compounds. Vacancies almost always occur next to Te atoms, which form one sublattice of the rock salt structure.

1. Introduction

Phase change materials (PCM) are the active components of the prominent rewritable storage media digital versatile disk (DVD-RW) and the Blu-ray Disc (BD-RE), and they are favored for future non-volatile computer memories, such as PC-RAM. Nanosized bits in a thin polycrystalline layer are switched reversibly and extremely rapidly between amorphous (*a*-) and crystalline (*c*-) states, which can be identified by measuring the resistivity or optical reflectivity. The search for materials that crystallize rapidly at temperatures below the melting point while retaining data for many years at room temperature has focused on narrow gap semiconductors (NGS) containing Te [1] and Sb: amorphous Te films crystallize spontaneously near 0 °C, and *a*-Sb at higher temperatures, so that the pure elements are inappropriate for PCM.

Popular compounds containing Te include Sb/Te alloys near the eutectic composition $Sb_{0.7}Te_{0.3}$, with small amounts of other elements (Ag, In in AIST [2], Ge in GeST), and the pseudobinary materials $(GeTe)_{1-x}(Sb_2Te_3)_x$ (GST) [3,4]. GST alloys provided the first practical PCM and have remained the standard over decades [5]. The crystallization processes in these two composition regions [Fig. 1(a)] differ: GST alloys (group 1) crystallize via nucleation [Fig. 1(b)], Sb/Te alloys near the eutectic composition (group 2) crystallize from the polycrystalline surroundings [Fig. 1(c)].

Amorphous GST alloys resist crystallization at room temperature, but order at higher temperatures to rock salt (RS, Fm3 m) structures, which show wide composition tolerance and are metastable over many years at archival temperatures. Vacancies (cavities) are crucial elements of the metastable structures, and Yamada [6] proposed that sites of the anion sublattice were occupied by Te atoms, and the cation sublattice randomly by Ge and Sb atoms and vacancies. Recent work has focused on "GeTe-rich" materials, such as the Blu-ray Disc material $Ge_8Sb_2Te_{11}$ ($x = 1/9$) [7]. Improved thermal stability and crystallization speed of *a*-Sb_2Te_3 followed alloying with scandium ($Sc_{0.2}Sb_2Te_3$, [8,9]) or yttrium $Y_xSb_{2-x}Te_3$ [10].

The following criteria are essential for PCM.

- Rapid write (amorphization) and read (crystallization) processes.
- Unambiguous property contrast between amorphous and crystalline states (reflectivity, conductivity).
- Cyclability, i.e. stability at operating temperatures (typically 100–150 °C) without phase separation or excessive power demands.

There have been countless studies of phase change properties in alloys of elements of groups 13–16, particularly those near the diagonal in the periodic table between B and Po. Why is it then that GST alloys near the GeTe-Sb_2Te_3 tie-line have dominated the discussion? This article outlines ways to think about this question and possible elements of an answer.

E-mail address: r.jones@fz-juelich.de.

[1] Presented as plenary lecture at 18th European Conference on Solid State Chemistry, Prague, Czech Republic, 11 July 2023.

https://doi.org/10.1016/j.solidstatesciences.2024.107524
Received 23 October 2023; Received in revised form 21 March 2024; Accepted 25 March 2024
Available online 21 April 2024

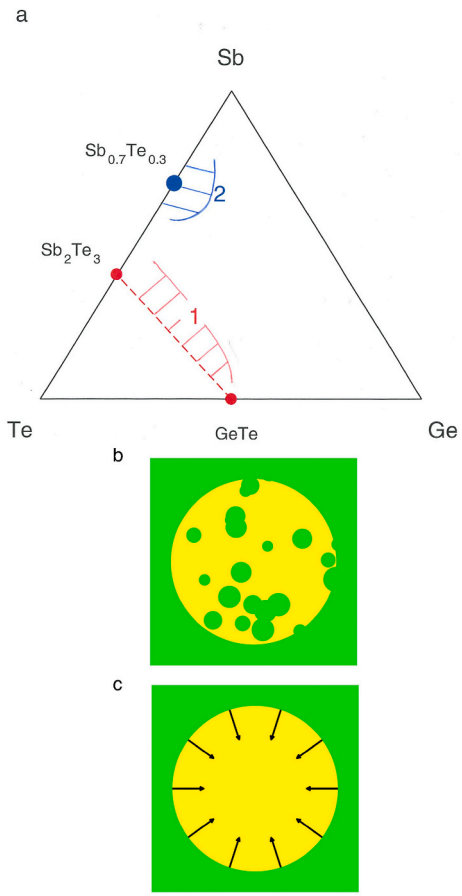

Fig. 1. (a) Compositions of Ge/Sb/Te alloys used in commercial PCM. (b) Crystallization mechanism in group 1 alloys (nucleation). (c) Crystallization mechanism in group 2 alloys (growth from polycrystalline surroundings).

In Sec. 2 we show that high-throughput deposition techniques have provided important information about the structure and properties of GST alloy films. We note the value of coordinate schemes in distinguishing between PCM, and discuss the valence orbitals and related properties in Ge, Sb, Te, and other atoms in groups 13–16. In Sec. 3, we discuss the structural instabilities associated with partially occupied nearly free electron (NFE) bands, and we discuss (Sec. 4) experimental information and simulations of crystallization of *a*-GST and a model for understanding the process. Our conclusions follow in Sec. 5. For further details and literature see Ref. [11]; general bonding concepts are reviewed in Refs. [12,13].

2. Structures, coordinate schemes, valence atomic orbitals

2.1. Structures, properties

Combinatorial methods have pervaded many areas of chemistry and biology over the past decades, enabling the preparation and screening of families ("libraries") of compounds. The techniques have been applied only recently to PCM, but the results have been impressive. The development of physical vapour deposition techniques has made it possible to scan a variety of properties of Ge/Sb/Te alloys [14,15]. The crystallization temperature T_c of an amorphous phase gives both a guide to the robustness of data storage and to the power requirements for phase switching; T_c for GST alloys is shown in Fig. 2 [15].

Only small regions of the composition diagram (Fig. 1) provide alloys with sufficiently low T_c, and the existence of a "crystallization valley" is unexpected and remarkable. This valley follows the line connecting Ge_2Te_3 with Sb_2Te_3, where Te atoms make up 60 % of the total

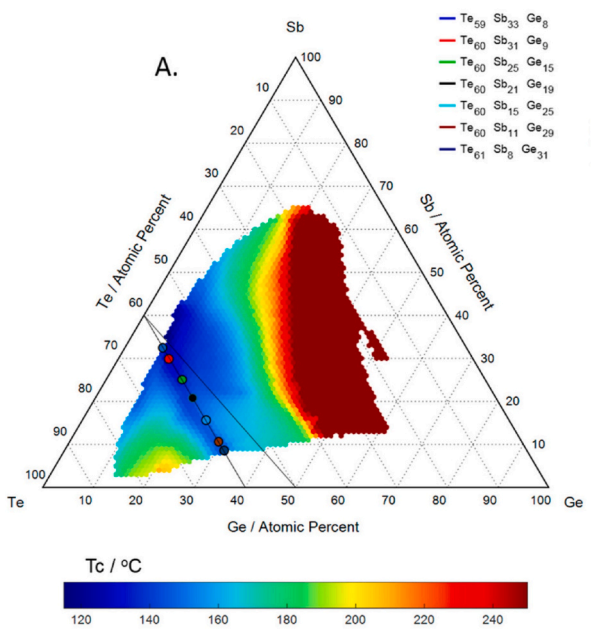

Fig. 2. Crystallization temperatures of GST alloys. Several compositions along the "crystallization valley" are shown. Reprinted with permission from Ref. [15]. Copyright 2017 American Chemical Society.

throughout, and not the GST tie-line $(GeTe)_{1-x}(Sb_2Te_3)_x$. Both tie-lines are shown in Fig. 2.

In Fig. 3 we show the change in optical reflectivity on crystallization. Again, only small regions of the composition diagram give satisfactory contrast. The reasons for this become clearer when we study the structures of GST-alloys determined by x-ray diffraction (Fig. 4). Many compositions remain amorphous above 200 °C, and others show segregation into mixed phases containing elemental Te, with obvious negative consequences for cyclability. In the region near the GST tie-line, two transitions can be observed: amorphous-to-cubic GST, and cubic-to-hexagonal GST structures [15], attributes of many successful PCM containing Ge, Sb, and Te.

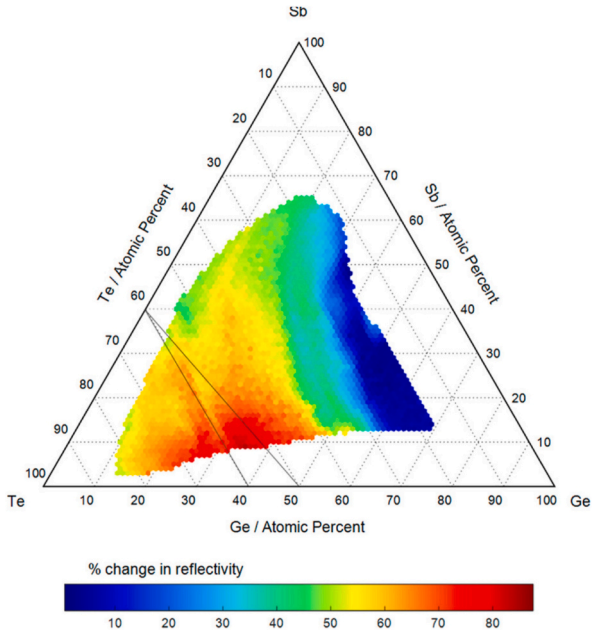

Fig. 3. Percentage change in optical reflectivity on crystallization. Reprinted with permission from Ref. [15]. Copyright 2017 American Chemical Society.

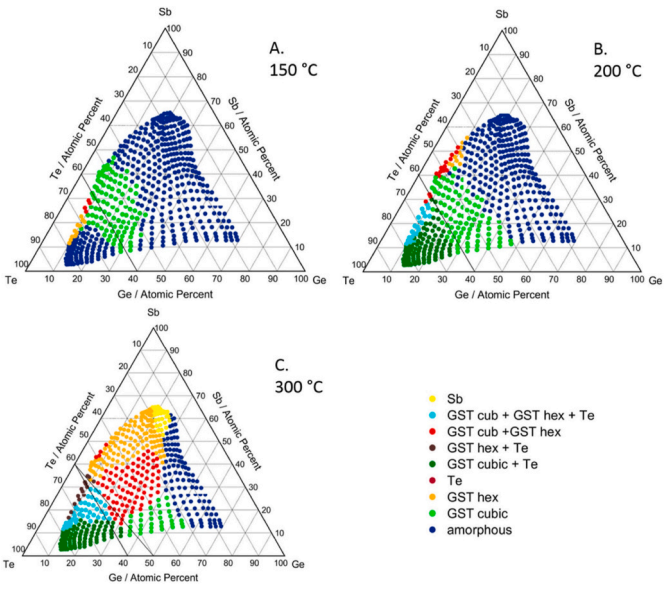

Fig. 4. Structures of Ge/Sb/Te alloys at 150, 200, and 300 °C. Reprinted with permission from Ref. [15]. Copyright 2017 American Chemical Society.

These high-throughput measurements provide a wealth of information that is invaluable for selecting potential candidates for PCM. Compositions near the "GeTe-rich" end of the GST tie-line, in particular, have clear advantages over other regions, although lower crystalline temperatures are found for compositions with higher Te concentrations near the Ge_2Te_3–Sb_2Te_3 tie-line.

2.2. Coordinate schemes

Trends in structures and other properties of elements and compounds can often be identified if plotted with appropriate variables (coordinates), a well-known example being the rows and columns of the periodic table. Elements to the left are metals, while most others are covalently bonded semiconductors and insulators, with a tendency to metallic behavior as the atomic number Z increases. Pauling [16] discussed the properties of atoms in terms of their location in the periodic table and defined their electronegativities in terms of bond energies of small molecules. Mulliken [17] defined electronegativity in purely *atomic* terms as the average of ionization energy and electron affinity, and our focus is also on the constituent atoms. Electronegativity schemes are reviewed in Ref. [18] and coordinate schemes in general in Refs. [11,19].

Discussions of structures of binary (AB) compounds often focus on the differences between the coordinates of A and B, such as the distances corresponding to the maxima of valence orbital functions [20]. Littlewood [21] showed that more ionic 14–16 compounds have the RS structure, less polar bonding leads to rhombohedral structures, and large covalent gaps to the orthorhombic structure. PCM often comprise several elements, but schemes for binary compounds can be adapted by replacing the multielement compound by an equivalent binary material. For example, Ge and Sb atoms in crystalline Ge/Sb/Te-materials occupy one sublattice of an RS structure, and a stoichiometrically averaged coordinate can be derived [22].

2.3. Atomic orbitals from density functional calculations

Valence atomic orbitals determine the "size" and electronegativity of an atom, and the relationships between orbital overlap, hybridization, and bond strength go back to the early days of the quantum theory of molecules [23,24]. The bond strength, in particular, is largest if the orbital overlap is a maximum. We focus here on trends in the s- and p-valence orbitals in groups 13–16 elements obtained from density functional (DF) calculations [25] using the Perdew-Burke-Ernzerhof (PBE) [26] approximation to the exchange-correlation energy. The all-electron (semi-relativistic) calculations treat the mass-velocity and Darwin terms explicitly; spin-orbit coupling effects are included perturbatively [27].

2.4. Orbital trends and secondary periodicity

Biron noted over 100 years ago [28] that many chemical and physical properties exhibited "secondary periodicity," a zigzag behavior superimposed on a smooth trend down a column of the periodic table, examples being the heats of formation of oxides and chlorides of groups 15, 16, and 17. Anomalously large ionization energies are evident in fourth row compounds [29] and in the s-d excitation energies and the s^2-s^1 ionization energies in group 15 ions [30]. Secondary periodicity [29,31] is associated with the stronger and shorter bonds that result from the incomplete screening by the 3d-electrons of the additional nuclear change in elements beyond Ga ($Z = 31$, "d-block contraction") and by the 4f-shell in elements beyond Tl ($Z = 81$). The latter effect had been observed in 1925 in crystallographic measurements of oxides and termed "lanthanide contraction" [32].

Most PCM comprise elements of groups 13–16, and almost all are near the diagonal in the periodic table between B and Po. The valence orbitals of groups 13, 15, and 16 are shown in Ref. [11] (Fig. SF1–3), and pairwise similarity of both s- and p- orbitals is evident in all four groups. The trends can be quantified in several ways, including the energy eigenvalues ε_{nl}, where the eigenvalue splitting between the s- and p-valence orbitals is one measure of the tendency of the atomic orbitals to form sp-hybrids and directed bonds [19]. These eigenvalues are given for groups 13–16 in Ref. [11] (Table 1 and Fig. SF4). The radii of the maxima in these orbitals or those derived from an atomic model potential have also been used [21,22,33].

We focus here on the first radial moment of the orbitals or the normalized expectation value of r with respect to the orbitals

$$\langle r\rangle_{nl} = \int dr\ r\ |rR_{nl}|^2 \Big/ \int dr\ |rR_{nl}|^2, \tag{1}$$

which probes an orbital over its entire range. The results are shown in Fig. 5 and Table 1. For Ge, Sb, and Te the values of $\langle r\rangle_{nl}$ are 20–30 % greater than the radii where $R_{nl}(r)$ is a maximum: Ge (0.93,1.17), Sb (1.00,1.24), Te (0.94,1.15) [Å, $l = 0, 1$].

Table 1
Moments $\langle r\rangle_0$ and $\langle r\rangle_1$ (Å) and the corresponding DF (Kohn-Sham) eigenvalues ε_0 and ε_1 (hartree) for s- and p valence orbitals of atoms of groups 13, 14, 15, and 16.

Group	Element	$\langle r\rangle_0$	$\langle r\rangle_1$	ε_0	ε_1
13	B	1.033	1.218	−0.347	−0.133
	Al	1.346	1.824	−0.285	−0.100
	Ga	1.240	1.812	−0.329	−0.095
	In	1.381	1.980	−0.302	−0.093
	Tl	1.311	2.039	−0.351	−0.087
14	C	0.832	0.953	−0.506	−0.194
	Si	1.145	1.479	−0.398	−0.150
	Ge	1.120	1.534	−0.431	−0.143
	Sn	1.265	1.728	−0.385	−0.132
	Pb	1.223	1.787	−0.443	−0.129
15	N	0.698	0.786	−0.686	−0.264
	P	1.003	1.256	−0.514	−0.203
	As	1.026	1.352	−0.533	−0.191
	Sb	1.178	1.545	−0.472	−0.178
	Bi	1.150	1.619	−0.532	−0.168
16	O	0.603	0.670	−0.881	−0.332
	S	0.897	1.096	−0.634	−0.258
	Se	0.950	1.219	−0.635	−0.240
	Te	1.104	1.414	−0.553	−0.219
	Po	1.088	1.494	−0.622	−0.207

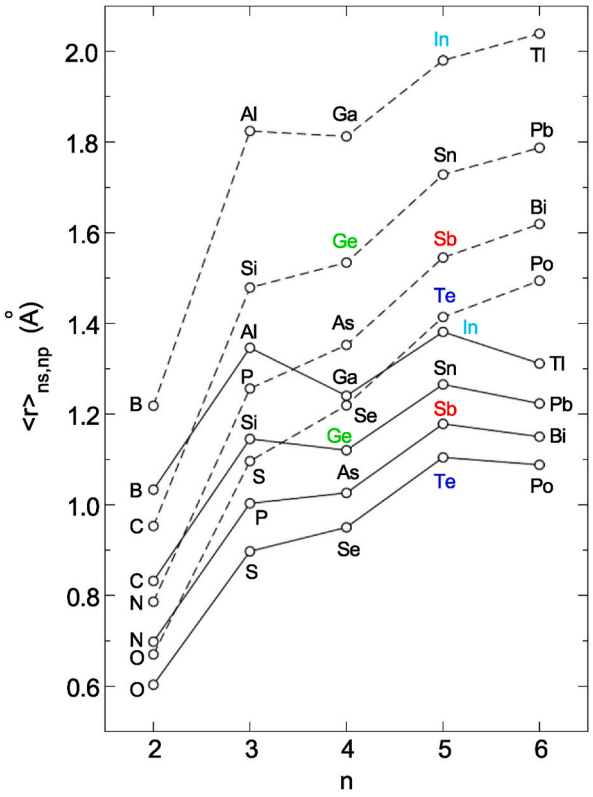

Fig. 5. First radial moments (Eq. (1)) for *s*- (solid curves) and *p*- (dashed curves) valence electrons in elements of groups 13–16. Reproduced with permission from Ref. [11]. Copyright 2020 American Physical Society.

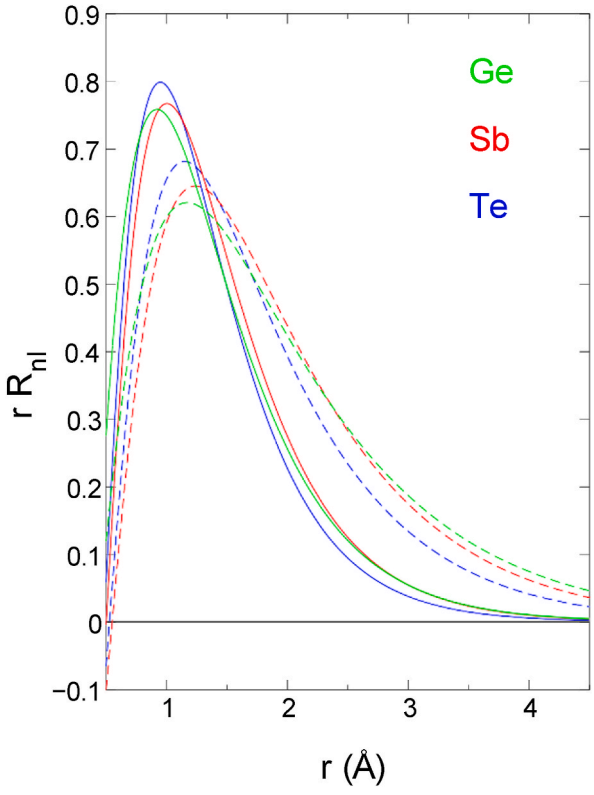

Fig. 6. Radial orbital functions rR_{nl} for *s*- (full curves) and *p*- (dashed curves) valence electrons in Ge (green), Sb (red), and Te (blue). Reproduced with permission from Ref. [11]. Copyright 2020 American Physical Society.

The first radial moments show that secondary periodicity is most pronounced in group 13 elements and more evident in *s*-orbitals than in *p*-orbitals. The structural consequences are immediate. The contraction of the 4*s* and 4*p*-orbitals in Ga is so large that they are more compact than the 3*s* and 3*p*-orbitals in Al (Fig. SF1 [11]), and the $^3\Sigma_u^-$ state is *shorter* in the dimer Ga_2 than in Al_2 [34]! The 3*p*-orbital in Si and the 4*p*-orbital in Ge (and the positions of their maxima) are very similar, and the 4*s*-orbital in Ge is even more compact than the 3*s*-orbital in Si.

The maxima in the 2*s*-and 2*p*-functions (Fig. SF5 [11]) and the corresponding moments (Table 1) are similar in the first row elements (B–F), and *sp*-hybridization is stronger. Carbon then has stronger and more flexible (single, double, and triple) bonds than in other group 14 elements, where the *p*-functions are significantly more diffuse than the *s*-functions and single bonds are favored [35]. Relativistic effects [31] in elements with $Z > 81$ lead to contraction of the orbitals of the innermost electrons and, by orthogonalization, to more compact *s*-valence orbitals with lower energy eigenvalues and weaker *sp*-hybridization. This is reflected in the cubic structures of PbS, PbSe, and PbTe.

The valence orbital functions for Ge, Sb, and Te (Fig. 6) and their moments are remarkably similar for elements with atomic numbers Z that range 32 (Ge) to 52 (Te). Orbital contraction on moving from left to right in the periodic table is counteracted by the tendency for orbitals to expand as the principal quantum number increases. The "size" of an atom provides an measure of the electronegativity of the elements, and the Pauling electronegativities in Ge (2.01), Sb (2.05), and Te (2.1) are almost identical [36]. The radial moment of the valence orbitals is one measure of size, and there is some evidence that "size" is more important than "electronegativity in explaining bonding in carbon halides [37].

3. Structural changes in GST – ingredients of a model

The most stable (trigonal) structures of Ge/Sb/Te alloys have never been used in commercial PCM, and the existence of the *metastable* RS structure is viewed as the "key" to their superior phase change properties [5]. The tie-line covers a wide range of compositions, and small departures from this line also lead to cubic structures.

Vacancies in GST are structural features [38], and their number maximizes the occupation of bonding *p*-orbitals [22,39], whose overlap is greatest for bond angles near 90° [23]. Cubic structures are often favored in such cases, and DF calculations indicated that cubic (*p*-bonding) structures are favored over chalcopyrite (sp^3-hybridized) structures in Te-based ternary PCM if the total occupancy of valence electrons $N_{sp} > 4.1$ [39].

3.1. Nearly free electron (NFE) model

Bloch [40] showed that the eigenfunctions of an electron in a periodic potential $V(\mathbf{r})$ can be written

$$\psi_{\mathbf{k}}(\mathbf{r}) = u_{\mathbf{k}}(\mathbf{r})\exp i(\mathbf{k}\cdot\mathbf{r}), \tag{2}$$

where $u_{\mathbf{k}}(\mathbf{r})$ has the periodicity of $V(\mathbf{r})$. If V vanishes [free-electron (FE) model], the eigenvalues are $E_{\mathbf{k}}(\mathbf{r}) = \hbar^2k^2/2\ m$, where $k = |\mathbf{k}|$. The reciprocal lattice points for a linear chain of periodicity a are the values of k where $\exp(ikx)$ has periodicity a, i.e. $g = n\pi/a$, where n is an integer. Peierls [41] showed that a gap in the band structure of $|2V_g|$ occurs at $k = g/2$ (Fig. 7), where V_g is the Fourier transform of V.

A periodic, three-dimensional potential $V(\mathbf{r})$ can be expanded as a Fourier series

$$V(\mathbf{r}) = \sum_{\mathbf{g}} V_{\mathbf{g}}\exp i(\mathbf{g}\cdot\mathbf{r}), \tag{3}$$

with

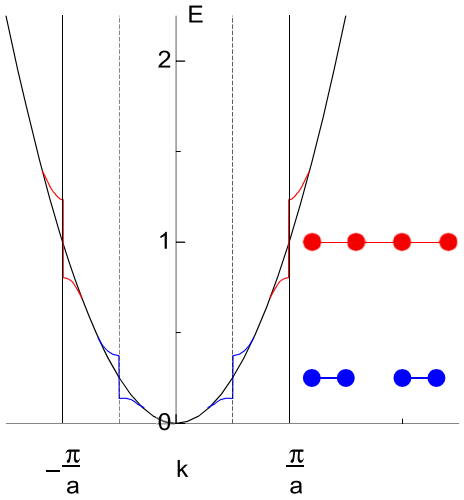

Fig. 7. Nearly free electron model of Peierls [41]. The red linear chain with equally spaced atoms and two electrons per atom has an energy gap (red) at $k = \pi/a$. If there is one electron per atom, a gap (blue) opens at $k = \pi/2a$ and the dimerized structure is more stable.

$$V_{\mathbf{g}} = \frac{1}{V}\int d\mathbf{r}\ V(\mathbf{r})\exp\ -i(\mathbf{g}\cdot\mathbf{r}). \tag{4}$$

Brillouin [42] showed how to construct polyhedral zones in two and three dimensions using planes bisecting each **g**-vector. Energy bands for values of **k** outside the smallest (first) Brillouin zone (BZ) can be folded into this zone to give the electronic band structure in the reduced zone scheme. If the structure has several atoms in the unit cell, $V_{\mathbf{g}}$ is replaced by $V_{\mathbf{g}}S_{\mathbf{g}}$, where the structure factor is

$$S_{\mathbf{g}} = \sum_{\mathbf{r}_i}\exp\ -i(\mathbf{g}\cdot\mathbf{r}_i). \tag{5}$$

and $\mathbf{r}_i$ are the coordinates of the atoms in the unit cell of volume V. $V_{\mathbf{g}}$ vanishes if $S_{\mathbf{g}}$ is zero, and the corresponding surfaces need not be counted as zone boundaries.

The FE and NFE models provide an excellent basis for studying metals and semiconductors. Mott and Jones [43, pp. 125–128] noted over 80 years ago that the conduction band widths measured in x-ray emission from many metals were close to the FE bandwidths calculated for the appropriate electron densities, and this is also true for many semiconductors. Fig. 8 shows FE bands for structures with the translational symmetry of the FCC lattice (includes the diamond and RS structures), together with the degeneracies of the bands and the Fermi energy E_F if there are 8 (diamond, Si, Ge) and 10 (Bi, GeTe) valence electrons in the unit cell. The large degeneracies of the bands near E_F in the case of 10 valence electrons suggest that there will be several bands near E_F derived from the FE bands along Λ and Q. The lower degeneracies and smaller value of E_F in the diamond structure imply fewer band crossings.

3.2. *Jones zones in extended* **k***-space, "Peierls distortion"*

A simple extension of the NFE model suggests a mechanism for structural distortions [44]. If we displace, for example, every second atom in a linear chain by the same amount, we double the size of the unit cell and can introduce gaps in the energy eigenvalue spectrum at half of the distance to the boundary of the original BZ [$\pm\pi/(2a)$] in Fig. 7. If this gap is at or near E_F, as in the case of a half-filled band, the distortion will be accompanied by a lower total energy. This mechanism, often referred to as the "Peierls distortion" [44], was applied much earlier by H. Jones to the 3D structure and other properties of the semimetal Bi [43,45,46].

If there are two or more electrons in the unit cell, the first band (and

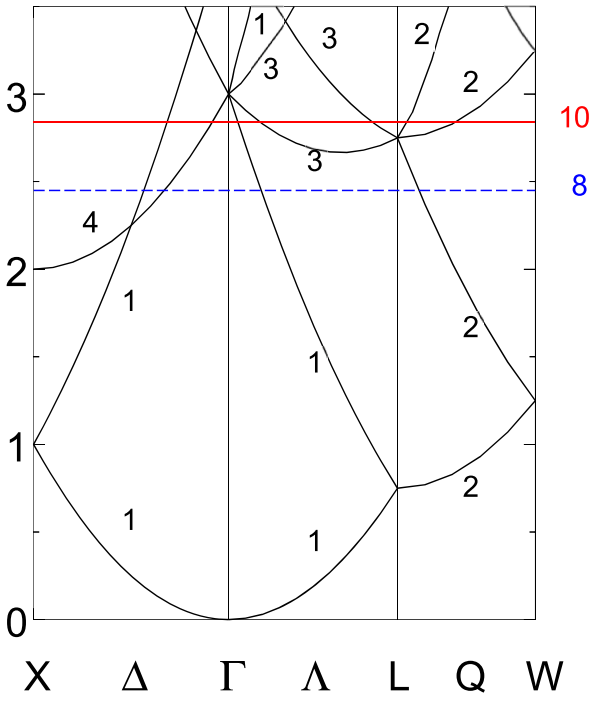

Fig. 8. Free-electron bands for structures with the translational periodicity of FCC lattices. X: 100, Γ: 000, L: $\frac{1}{2}\frac{1}{2}\frac{1}{2}$, W: $1\frac{1}{2}0$ [in units of $(2\pi/a)$, where a is the lattice constant]. Energies in units of $(2\pi/a)^2$. Also shown are the band degeneracies and the Fermi energies corresponding to 8 (blue, dashed) and 10 (red, solid) valence electrons in the unit cell. Reproduced with permission from Ref. [11]. Copyright 2020 American Physical Society.

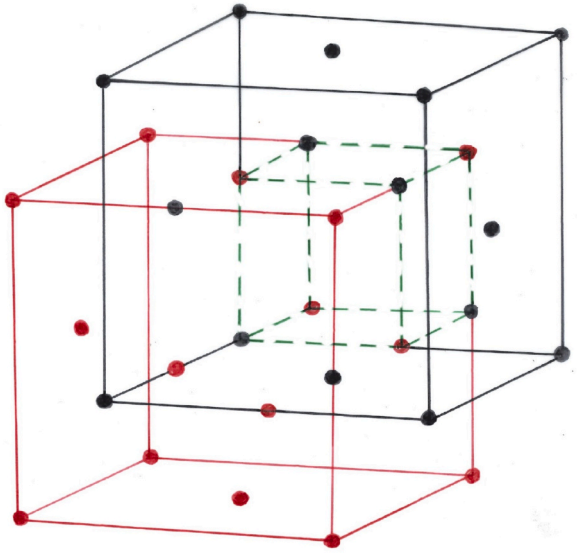

Fig. 9. SC structure (green, dashed) represented as two FCC lattices (red, black) displaced by half of the body diagonal of the latter. Reproduced with permission from Ref. [11]. Published by American Physical Society.

BZ) are occupied, and it is convenient to discuss the bands near E_F using the *extended* zone scheme. The group 15 elements As, Sb, and Bi have five valence electrons per atom and are metallic in the SC structure, which can be represented (Fig. 9) as two FCC lattices displaced by half of the body diagonal. Two small distortions lead to the *A*7 (rhombohedral) structure found in these three elements. The RS and rhombohedral structures of GeTe are related in the same way. In this picture, the *A*7 structure of Bi is simply a consequence of the instability inherent in an

SC structure with half-filled bands. The distortion, which decreases in the order As → Sb → Bi as *sp*-hybridization weakens, yields a structure with shorter and longer bonds.

The structures of As, Sb, Bi, and GeTe have two atoms and 10 valence electrons in the unit cell, so that at least five BZ are occupied. The fifth BZ is complex [Fig. 10(left)], and Jones adopted an alternative zone bounded by planes corresponding to large values of $S_{\mathbf{g}}$. The "Jones zones" for 10 electrons [trigonal, Fig. 10(right)] has six planes arising from reciprocal lattice vectors of the form [11 0] and six from vectors related to [221]. It is much simpler than the fifth BZ, but it has the same volume and contains five states per atom. The small number of $V_{\mathbf{g}}$ and the presence of parallel zone faces give rise to pairs of bands that are nearly parallel in a significant volume of **k**-space and give rise to characteristic peaks and shoulders in the optical properties.

The form of the FE bands near E_F suggests that valence band occupancies close to 10 will have overlapping bands and semimetallic properties. Jones [43,45] focused on the Landau-Peierls diamagnetism and explained the rhombohedral structure of Bi, where the valence and conduction bands overlap. The electron and hole pockets in the Fermi surface are consistent with the high diamagnetism and low (semimetallic) conductivity of Bi, as well as As and Sb. In GeTe, the rhombohedral form is a narrow-gap semiconductor.

The Jones zone construction has also provided insight into the electronic structure and optical properties of the semiconductors Si and Ge [12,47] and has been applied to several other materials with average valence 5, including SnTe [48]. Nevertheless, the model of Jones has largely been ignored in the PCM field, where structural changes are usually attributed to the "Peierls distortion", a one-dimensional concept.

The band structure calculations of As, Sb, and Bi by Cohen et al. [49] showed a valence band of predominantly *p*-bonding character separated from *p*-antibonding bands that are mostly unoccupied. Mixing of bonding and antibonding character and *sp*-hybridization occur, and the location of the few holes in the uppermost valence band and the few electrons in lowest conduction band are determined by these mixings. It was confirmed much later that the distortions led to an NGS and to a transition to a semimetal by a mechanism "consistent with the Jones-Peierls model" [50]. The main features of the band structure are a hole pocket near T and an electron pocket near L, where both T and L are derived from the point L for FE bands for 10 electrons in the FCC unit cell (Fig. 8). Conduction and valence band extremities in GeTe, SnTe, PbS, PbSe, and PbTe are also at or near L [51,52].

3.3. Ostwald's step rule for crystallization

GST is a supercooled liquid at 600 K. The history of metastable structure formation in liquids began in the 19th century with the work of Ostwald [53], who summarized his observations of crystallization with his *Stufensatz* ('step rule' or 'rule of stages'): for a metastable (or unstable) liquid that can crystallize in several forms, the first stage of nucleation is to the metastable form nearest in free energy, not to the most stable form (Fig. 11). A refinement by Stranski and Totomanow

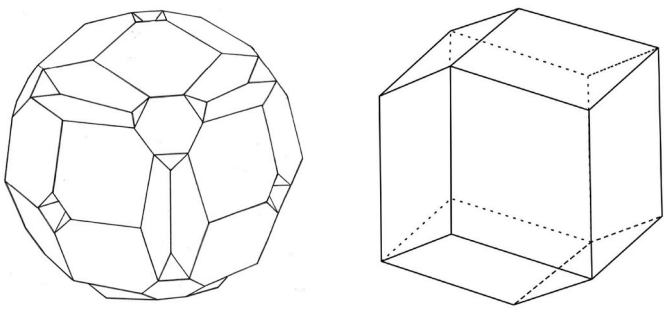

Fig. 10. (left) Fifth Brillouin zone of FCC structure and (right) Jones zone of the bismuth (*A*7) structure.

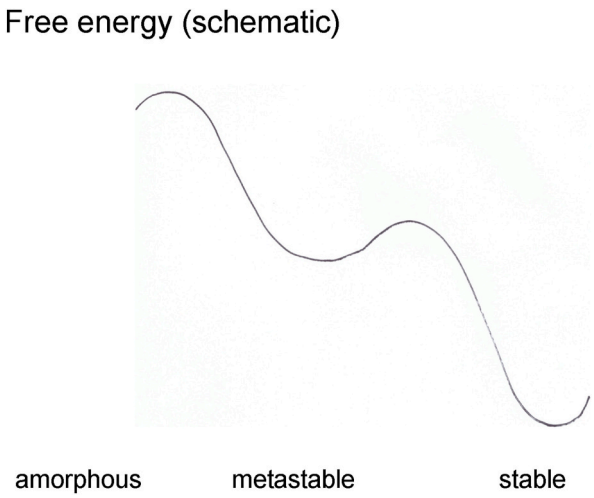

Fig. 11. Schematic variation of free energy during crystallization via an intermediate (metastable) structure.

[54] focused on the metastable form that is separated from the initial state by the lowest free energy *barrier*. This opens the prospect of finding multistep paths to the most stable form involving a variety of structures (polymorphs), and crystallization in the presence of multiple metastable intermediate phases has been studied extensively [55, and references therein].

Neither Ostwald's step rule nor the Stranski-Totomanov extension holds universally [56,57], but van Santen [58] used irreversible thermodynamics to show that a multiple-step reaction leads to an entropy production that is lower than in the direct reaction. Simulations [59] have shown that pathways for homogeneous nucleation could differ markedly from classical nucleation theory and follow a *microscopic* version of Ostwald's rule. The presence of a metastable liquid-liquid critical point lowers the free energy barrier and increases the nucleation rate during the crystallization of multicomponent systems [60].

4. Crystallization in GST

4.1. Results of simulations and experiment

Density functional simulations [61–63] of amorphous and liquid (ℓ)-GeTe and GST show the presence of vacancies and *ABAB*-rings (*A*: Ge, Sb, *B*: Te) in all phases. In *a*-GST, the distributions of Te–Sb–Te and Te-Ge-Te bond angles show definite peaks around 90°, and the dihedral angles for Ge–Te and Sb–Te bonds show maxima around 0, 90°, and 180° that also arise in cubic structures. Simulations of crystallization of *a*-GST [64–67] showed that *ABAB* rings reorient to the metastable RS structure [6] with Te atoms on the anion sublattice and an apparently disordered arrangement of Ge, Sb, and vacancies on the other. The vibration frequencies of GST (typically 3 THz [62]) allow several thousand vibrations on the scale of nanoseconds, and energy minimization leads to a dramatic reduction in the number of "wrong bonds" (Ge–Ge, Ge–Sb, Sb–Sb, Te–Te). Te atoms order rapidly in the anion sublattice, but slower ordering of the other elements and vacancies also occurs. Overall, Ge and Sb atoms move away from vacancies, which accumulate in the neighborhood of Te atoms. The distribution of vacancies around Te atoms found in the simulations agrees well with the results of ^{125}Te nuclear magnetic resonance studies [68].

Fig. 12 (lower) shows a snapshot of the ordered structure of GST in Ref. [65], where the cation lattice shows clear signs of segregation. "Ge-rich" and "Sb-rich" layers in the ordered structure contain approximately 60 % of the majority. Vacancies are absent in the Te layers, show a strong preference for Te as nearest neighbors, and are more common in Ge-rich layers than in Sb-rich layers. The time dependence of the associated partial pair distribution functions and coordination numbers

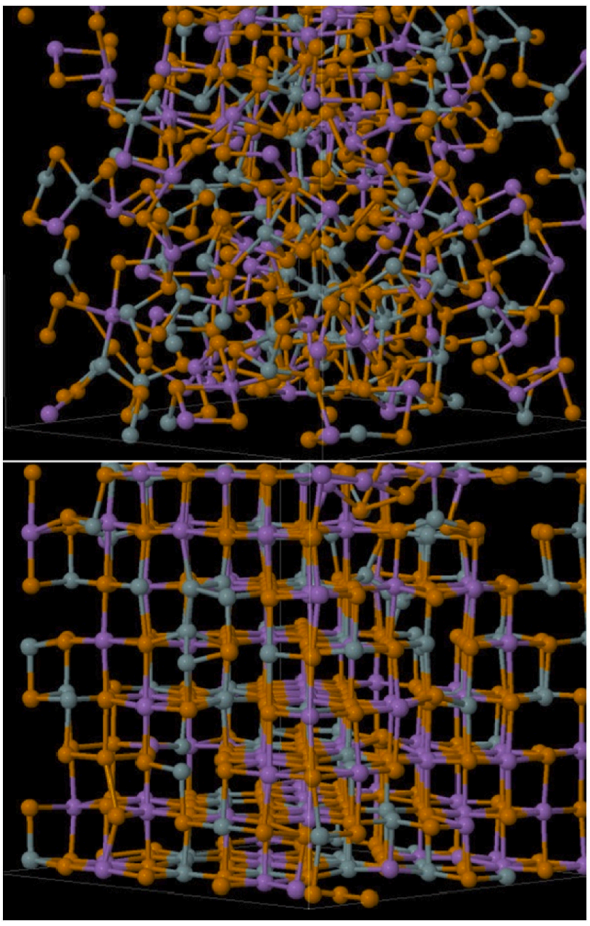

Fig. 12. Structures of (upper) amorphous and (lower) (metastable) crystalline GST determined by DF/MD simulations [66]. Orange: Te, grey: Ge, purple: Sb. Ordering in the Te layers is almost complete. Segregation is evident in other layers.

confirm this ([65], including Supplementary Information, [66]). STEM measurements and DF calculations [69] show that further annealing results in vacancy segregation into (111) planes of the trigonal structure discussed above.

4.2. Model

The main driving force for structural changes in GST is the energy lowering accompanying the occupation of bonding orbitals, and the number of vacancies in the metastable RS phases of the PCM $(GeTe)_{1-x}(Sb_2Te_3)_x$ is such that that all bonding p-orbitals are occupied [39]. It is common to associate p^3-configurations with cubic structures, and an SC structure, viewed as two FCC lattices displaced along the cubic diagonal (Fig. 9), is unstable against a combined trigonal shear and rhombohedral distortion. This occurs in the elements As, Sb, and Bi; the GeTe structure is rhombohedral at room temperature and RS at high temperatures. These materials have five valence electrons (s^2p^3) per atom, and Jones [45] explained the structure and semimetallic properties of Bi using the approach described above. The number of valence electrons in the pseudobinary PCM mentioned above is close to five (4.71 in $Ge_1Sb_4Te_7$, $x = 2/3$; 4.91 in $Ge_8Sb_2Te_{11}$, $x = 1/9$).

The similarity of the s- and p-valence orbitals in Ge, Sb, and Te atoms is a direct consequence of "secondary periodicity." The "d-block contraction" of the valence orbitals of Ge balances the orbital contraction found in Sb (group 15) and Te (group 16) to the right of Ge in the periodic table. The principle of maximum overlapping then implies that the energy lowering in GST will be greater than in other combinations of atoms of the same groups.

These observations allow us to consider a model for the crystallization of a-GST, where the structure has many cubic features. If we focus on the cubic aspects alone, assume that the orbitals of Ge, Sb, and Te are *identical*, and that the GST systems have an *average* of five valence electrons (s^2p^3) per site, including vacancies, we can adapt the arguments applied by Jones to Bi [45] to rationalize the metastable RS structures found in Ge/Sb/Te alloys. The structural changes must also reflect the composition and the different electronic configurations and valences of the components, Ge $3s^23p^2$, Sb $4s^24p^3$, Te $4s^24p^4$, and vacancies s^0p^0. The most stable average configuration (s^2p^3) can be maintained if Sb and particularly Ge atoms move away from vacancies, which accumulate near Te atoms. These trends are seen clearly in the simulations, where Ge atoms are also more mobile than Sb, and very few vacancies have Ge or Sb atoms as neighbors in the ordered metastable structure [65]. Te atoms make up at least half of the total number in all Ge/Sb/Te alloys near the tie-line, and attainment of an average configuration of s^2p^3 with these constraints will favor a Te sublattice.

The formation of a metastable state well above the energy of the most stable (trigonal) structure is an example of Ostwald's step rule in a multicomponent system. The free energy is lowered by the distortion to the RS structure with the most rapid kinetics. The accompanying process to the most stable structure is much slower, but the early stages of order—the segregation of Ge and Sb atoms—are evident in DF/MD simulations (Fig. 12).

5. Concluding remarks

The requirements of PCM are satisfied to varying extents by many compounds of elements of groups 14, 15, and 16, but almost all commercial products use alloys containing Ge, Sb, and Te. The time-limiting step in the read-write cycle is crystallization of amorphous bits, which is driven by the lowering of energy on bond formation. This is greatest when the overlap of the valence orbitals is maximized, which occurs in Ge, Sb, and Te (see Sec. 2.4); Sb and Te are adjacent in the periodic table, and the d-block contraction in Ge counteracts the expansion usually associated with elements in a column to the left. This contraction is evident in germanium chalcogenides. The bond lengths in the most stable ($^1\Sigma_g$) states of the diatomic molecules are: GeO 1.625 Å, GeS 2.012 Å, GeSe 2.135 Å, GeTe 2.340 Å [70]; germanium monoxide GeO is not a stable compound [71], crystalline GeS and GeSe have the same structure (orthorhombic) and similar nearest neighbour separations (2.47 Å and 2.56 Å, respectively), while the Ge–Te separation in rock salt GeTe is much larger (3.00 Å) [72].

Valence orbitals are characterized here by their radial moments (Fig. 5, Table 1), and choosing elements with comparable values results in materials with small charge transfer between the atoms. Secondary periodicity is evident in the orbital moments (Fig. 5) and in eigenvalue plots (Fig. SF4 of [11]), where variations with Z are less pronounced. Both provide guides to finding replacements for Ge, Sb, and Te in PCM.

Si provides a good match to Ge, but its sp-splitting is smaller, and hybridization is more pronounced. Se and As, like Ge, are subject to the d-block contraction, and the overlap of their orbitals with those of Ge is less than for Te and Sb, respectively. The short half-life of all Po isotopes rules it out as a replacement for Te, and Bi shares with Po and other elements with $Z > 80$ a pronounced relativistic contraction of the s-orbital, weak sp-hybridization, and a tendency to favor cubic over rhombohedral structures. The replacement of a fraction of Sb by Bi or Ge by Sn may still be favorable.

There have been numerous attempts to rationalize the behavior of PCM and other narrow gap semiconductors comprising elements near the diagonal of the periodic table between B and Po. Pauling and others refer to these elements as *metalloids*, which have "… properties intermediate between those of metals and those of non-metals" [73, p. 612]. It has been proposed that the function of PCM reflects drastic changes in the nature of the chemical bond in the two phases: "resonant bonding" in

the crystal [74], transient three-center bonds mediated by lone pair electrons [75], or "metavalent bonding" in "incipient metals" [76,77]. Alignment of *p*-orbitals in the ordered structure has been invoked as a requirement for large optical contrast in PCM [78]. The identification of particular bonding mechanisms is often difficult, and the topic remains controversial [79,80].

We have focused here on the relationship between the structure and the *number* of valence electrons of the component atoms, the extent of their orbitals as characterized by the radial moments, the NFE band structure in the extended zone scheme, and the composition of the materials. All aspects are important, and the focus is broader than requiring an average count of 3 *p*-electrons per site [22,39]. In the context of materials with average valence 5, Cohen et al. [49] concluded that the "band" (reciprocal space) picture provides a "deeper basis for understanding" than the "bond" (real space) perspective.

The NFE approach is the basis of the structural distortion models developed by Jones in 1934 and by Peierls in 1955, and it is close in spirit to the density functional formalism [25] used in most PCM simulations. Dramatic changes in electronic and structural properties can result without invoking different bonding mechanisms; in bulk Al and Si, for example, a different number of valence electrons can lead to an FCC metal or a semiconductor with a diamond structure and a gap of over 1 eV. Large changes can also occur in Ge/Sb/Te materials, where the actual *mechanism* of bonding in their different phases is a lowering of kinetic energy due to wave function overlap [12,81] with only differences in detail. We have emphasized the *structures* involved, particularly the presence of a metastable structure accessible at moderate temperatures from the disordered state. This is a crucial property of alloys along the GST tie-line.

CRediT authorship contribution statement

Robert O. Jones: Conceptualization, Investigation, Writing – review & editing, Writing – original draft.

Declaration of competing interest

The authors declare that they have no known competing financial interests or personal relationships that could have appeared to influence the work reported in this paper.

Data availability

No data was used for the research described in the article.

Acknowledgements

I thank J. Akola and J. Kalikka for collaboration on Ge/Sb/Te simulations over many years. Computer time provided by the JARA-HPC Vergabegremium on the JARA-HPC partition of the supercomputers JUQUEEN and Jureca (Forschungszentrum Jülich) is acknowledged gratefully.

References

[1] M. Takenaga, N. Yamada, S. Ohara, K. Nishiuchi, M. Nagashima, T. Kashihara, S. Nakamura, T. Yamashita, New optical erasable medium using tellurium suboxide thin film, Proc. SPIE-Int. Soc. Opt. Eng. 420 (1983) 173–177.
[2] T. Matsunaga, J. Akola, S. Kohara, T. Honma, K. Kobayashi, E. Ikenaga, R.O. Jones, N. Yamada, M. Takata, R. Kojima, From local structure to nanosecond recrystallization dynamics in AgInSbTe phase-change materials, Nat. Mater. 10 (2011) 129–134.
[3] N. Yamada, E. Ohno, N. Akahira, K. Nishiuchi, K. Nagata, M. Takao, High speed overwritable phase change optical disk material, Jpn. J. Appl. Phys. 26 (1987) 61.
[4] T. Matsunaga, N. Yamada, Crystallographic studies on high-speed phase-change materials used for rewritable optical recording disks, Jpn. J. Appl. Phys. 43 (2004) 4704–4712.
[5] N. Yamada, Origin, secret, and application of the ideal phase-change material GeSbTe, Phys. Status Solidi B 249 (2012) 1837–1842.
[6] N. Yamada, Erasable phase-change optical materials, MRS Bull. 21 (1996) 48–50.
[7] J. Akola, R.O. Jones, Structure of amorphous $Ge_8Sb_2Te_{11}$: GeTe-Sb_2Te_3 alloys and optical storage, Phys. Rev. B 79 (2009) 134118.
[8] F. Rao, K. Ding, Y. Zhou, Y. Zheng, M. Xia, S. Lv, Z. Song, S. Feng, I. Ronneberger, R. Mazzarello, W. Zhang, E. Ma, Reducing the stochasticity of crystal nucleation to enable subnanosecond memory writing, Science 358 (2017) 1423–1427.
[9] J. Akola, R.O. Jones, Speeding up crystallization, Science 358 (2017) 1386, 1386.
[10] Y. Zhou, L. Sun, G.M. Zewdie, R. Mazzarello, V.L. Deringer, E. Ma, W. Zhang, Bonding similarities and differences between Y-Sb-Te and Sc-Sb-Te phase-change memory materials, J. Mater. Chem. C 8 (2020) 3646–3654.
[11] R.O. Jones, Phase change memory materials: rationalizing the dominance of Ge/Sb/Te alloys, Phys. Rev. B 101 (2020) 024103.
[12] R.O. Jones, Bonding in phase change materials: concepts and misconceptions, J. Phys. Condens. Matter 30 (2018) 153001.
[13] R.O. Jones, The chemical bond in solids – revisited, J. Phys. Condens. Matter 34 (2022) 343001.
[14] S. Guerin, B.E. Hayden, Physical vapor deposition method for the high-throughput synthesis of solid-state material libraries, J. Comb. Chem. 8 (2006) 66–73.
[15] S. Guerin, B. Hayden, D.W. Hewak, C. Vian, Synthesis and screening of phase change chalcogenide thin film materials for data storage, ACS Comb. Sci. 19 (2017) 478–491.
[16] L. Pauling, The Nature of the Chemical Bond, third ed., Cornell University Press, Ithaca, N.Y., 1960.
[17] R.S. Mulliken, A new electroaffinity scale; together with data on valence states and on valence ionization potentials and electron affinities, J. Chem. Phys. 2 (1934) 782–793.
[18] G.D. Sproul, Evaluation of electronegativity scales, ACS Omega 5 (2020) 11585–11594.
[19] P.B. Littlewood, Structure and bonding in narrow gap semiconductors, CRC Crit. Rev. Solid State Mater. Sci. 11 (1983) 229–285.
[20] A. Zunger, M.L. Cohen, First-principles nonlocal-pseudopotential approach in the density-functional formalism. II. Application to electronic and structural properties of solids, Phys. Rev. B 20 (1979) 4082–4108.
[21] P.B. Littlewood, The crystal structure of IV-VI compounds. I. Classification and description, J. Phys. C Solid State Phys. 13 (1980) 4855–4873.
[22] D. Lencer, M. Salinga, B. Grabowski, T. Hickel, J. Neugebauer, M. Wuttig, A map for phase-change materials, Nat. Mater. 7 (2008) 972–977.
[23] J.C. Slater, Directed valence in polyatomic molecules, Phys. Rev. 37 (1931) 481–489.
[24] L. Pauling, The Nature of the Chemical Bond. Application of results obtained from the quantum mechanics and from a theory of paramagnetic susceptibility to the structure of molecules, J. Am. Chem. Soc. 53 (1931) 1367–1400.
[25] R.O. Jones, Density functional theory: its origins, rise to prominence, and future, Rev. Mod. Phys. 87 (2015) 897–923.
[26] J.P. Perdew, K. Burke, M. Ernzerhof, Generalized gradient approximation made simple, Phys. Rev. Lett. 77 (1996) 3865–3868.
[27] J.H. Wood, A.M. Boring, Improved Pauli Hamiltonian for local-potential problems, Phys. Rev. B 18 (1978) 2701–2711. The large component radial orbital is solved explicitly in the self-consistent cycle, and the small component is determined from it by perturbation theory.
[28] E.V. Biron, The phenomenon of secondary periodicity, Zh. Russ. Fiz.-Khim. Obshch. 47 (1915) 964–988.
[29] S.A. Shchukarev, The periodic law of D. I. Mendeleev as a basic concept in modern chemistry, J. Gen. Chem. USSR 25 (1954) 595–603.
[30] R.S. Nyholm, Electron configuration and structure of transition-metal complexes, Proc. Chem. Soc. 1961 (1961) 273–296.
[31] P. Pyykkö, Relativistic effects in structural chemistry, Chem. Rev. 88 (1988) 563–594. And references therein.
[32] V.M. Goldschmidt, T. Barth, G. Kunde, Geochemische Verteilungsgesetze der Elemente V. Isomorphie und Polymorphie der Sesquioxyde. Die Lanthanum-Kontraktion und ihre Konsequenzen, Norsk. Vid. Akad. Skr. 1, M.-N. Kl. 7 (1925) 1–59.
[33] J. St John, A.N. Bloch, Quantum-defect electronegativity scale for nontransition elements, Phys. Rev. Lett. 33 (1974) 1095–1098.
[34] R.O. Jones, Simulated annealing study of neutral and charged clusters: al_n and Ga_n, J. Chem. Phys. 99 (1993) 1194–1206.
[35] J. Harris, R.O. Jones, Bonding trends in the group-IV A dimers C_2-Pb_2, Phys. Rev. 19 (1979) 1813–1818.
[36] ? See https://en.wikipedia.org/wiki/Electronegativity retrieved on 14 September 2023.
[37] E. Blokker, X. Sun, J. Poater, J.M. van der Schuur, T.A. Hamlin, F.M. Bickelhaupt, The chemical bond: when atom size instead of electronegativity difference determines trend in bond strength, Chem. Eur J. 27 (2021) 15616–15622.
[38] J. Robertson, K. Xiong, P. Peacock, Electronic and atomic structure of $Ge_2Sb_2Te_5$ phase change memory material, Thin Solid Films 515 (2007) 7538–7541.
[39] M. Luo, M. Wuttig, The dependence of crystal structure of Te-based phase-change materials on the number of valence electrons, Adv. Mater. 16 (2004) 439–443.
[40] F. Bloch, Über die Quantenmechanik der Elektronen in Kristallgittern, Z. Phys. 52 (1929) 555–600.
[41] R. Peierls, Zur Theorie der elektrischen und thermischen Leitfähigkeit von Metallen, Ann. Phys.-Berlin 396 (1930) 121–148.
[42] L. Brillouin, Les électrons libre dans les métaux et le role des reflexions de Bragg, J. Phys. Radium 1 (1930) 377–400.
[43] N.F. Mott, H. Jones, The Theory of the Properties of Metals and Alloys, Clarendon Press, Oxford, 1936.
[44] R.E. Peierls, Quantum Theory of Solids, Clarendon Press, Oxford, 1955.

[45] H. Jones, Applications of the bloch theory to the study of alloys and of the properties of bismuth, P. R. Soc. A 147 (1934) 396–417.
[46] H. Jones, The Theory of Brillouin Zones and Electronic States in Crystals, second, revised ed., 1975. North-Holland, Amsterdam.
[47] V. Heine, R.O. Jones, Electronic band structure and covalency in diamond-type semiconductors, J. Phys. C Solid State Phys. 2 (1969) 719–732.
[48] Y. Onodera, Band structure and Jones zone of SnTe, Solid State Commun. 11 (1972) 1397–1399.
[49] M.H. Cohen, L.M. Falicov, S. Golin, Crystal chemistry and band structures of the group V semimetals and the IV-VI semiconductors, IBM Journal 8 (1964) 215–227.
[50] A.B. Shick, J.B. Ketterson, D.L. Novikov, A.J. Freeman, Electronic structure, phase stability, and semimetal-semiconductor transitions in Bi, Phys. Rev. B 60 (1999) 15484–15487.
[51] F. Herman, R.L. Kortum, I.B. Ortenburger, J.P. Van Dyke, Relativistic band structure of GeTe, SnTe, PbTe, PbSe, and PbS, J. Phys. Colloq. 29 (1968) 62–77.
[52] H.M. Polatoglou, G. Theodorou, N.A. Economou, Band structure of cubic and rhombohedral GeTe, in: E. Gornik, H. Heinrich, L. Palmetshofer (Eds.), Physics of Narrow Gap Semiconductors, Springer, Berlin, Heidelberg, 1982, pp. 221–225.
[53] W. Ostwald, Studien über die Bildung und Umwandlung fester Körper. 1. Übersättigung und Überkühlung, Z. Phys. Chem. 22 (1897) 289–330.
[54] I.N. Stranski, D. Totomanow, Keimbildungsgeschwindigkeit und Ostwaldsche Stufenregel, Z. Phys. Chem. 163 (1933) 399–408.
[55] M. Santra, R.S. Singh, B. Bagchi, Nucleation of a stable solid from melt in the presence of multiple metastable intermediate phases: wetting, Ostwald's step rule, and vanishing polymorphs, J. Phys. Chem. B 117 (2013) 13154–13163.
[56] T. Threlfall, Structural and thermodynamic explanations of Ostwald's rule, Org. Process Res. Dev. 7 (2003) 1017–1027.
[57] L.O. Hedges, S. Whitelam, Limit of validity of Ostwald's rule of stages in a statistical mechanical model of crystallization, J. Chem. Phys. 135 (2011) 164902.
[58] R.A. van Santen, The Ostwald step rule, J. Phys. Chem. 88 (1984) 5768–5769.
[59] P.R. ten Wolde, D. Frenkel, Homogeneous nucleation and the Ostwald step rule, Phys. Chem. Chem. Phys. 1 (1999) 2191–2196.
[60] P. Wen, P. Harrowell, C.A. Angell, Fast and slow components in the crystallization of a model multicomponent system, $NaKCa(NO_3)$: the role of composition fluctuations, J. Phys. Chem. A 115 (2011) 6260–6268.
[61] J. Akola, R.O. Jones, Structural phase transitions on the nanoscale: the crucial pattern in the phase-change materials $Ge_2Sb_2Te_5$ and GeTe, Phys. Rev. B 76 (2007) 235201.
[62] J. Akola, R.O. Jones, Density functional study of amorphous, liquid and crystalline $Ge_2Sb_2Te_5$: homopolar bonds and/or AB alternation? J. Phys. Condens. Matter 20 (2008) 465103.
[63] J. Akola, R.O. Jones, Binary alloys of Ge and Te: order, voids, and the eutectic composition, Phys. Rev. Lett. 100 (2008) 205502.
[64] J. Kalikka, J. Akola, J. Larrucea, R.O. Jones, Nucleus-driven crystallization of amorphous $Ge_2Sb_2Te_5$: a density functional study, Phys. Rev. B 86 (2012) 144113.
[65] J. Kalikka, J. Akola, R.O. Jones, Simulation of crystallization in $Ge_2Sb_2Te_5$: a memory effect in the canonical phase-change material, Phys. Rev. B 90 (2014) 184109.
[66] J. Kalikka, J. Akola, R.O. Jones, Crystallization processes in the phase change material $Ge_2Sb_2Te_5$: unbiased density functional/molecular dynamics simulations, Phys. Rev. B 94 (2016) 134105.
[67] I. Ronneberger, W. Zhang, H. Eshet, R. Mazzarello, Crystallization properties of the $Ge_2Sb_2Te_5$ phase-change compound from advanced simulations, Adv. Funct. Mater. 25 (2015) 6407–6413.
[68] S. Sen, T.G. Edwards, J.-Y. Cho, Y.-C. Joo, Te-centric view of the phase change mechanism in Ge-Sb-Te alloys, Phys. Rev. Lett. 108 (2012) 195506.
[69] B. Zhang, W. Zhang, Z. Shen, Y. Chen, J. Li, S. Zhang, Z. Zhang, M. Wuttig, R. Mazzarello, E. Ma, X. Han, Element-resolved atomic structure imaging of rocksalt $Ge_2Sb_2Te_5$ phase-change material, Appl. Phys. Lett. 108 (2016) 191902.
[70] K.-P. Huber, G. Herzberg, Molecular Spectra and Molecular Structure. IV. Constants of Diatomic Molecules, Van Nostrand Reinhold, New York, 1979.
[71] M. Hoch, H.L. Johnston, The germanium–oxygen system, J. Chem. Phys. 22 (1954) 1376–1377.
[72] P. Villars (Ed.), Springer Materials (Online); PAULING FILE in: Inorganic Solid Phases, Springer-Verlag, Heidelberg, 2023.
[73] L. Pauling, General Chemistry, third ed., Freeman, San Francisco, 1970.
[74] K. Shportko, S. Kremers, M. Woda, D. Lencer, J. Robertson, M. Wuttig, Resonant bonding in crystalline phase-change materials, Nat. Mater. 7 (2008) 653–658.
[75] A. Kolobov, P. Fons, J. Tominaga, Understanding phase-change memory alloys from a chemical perspective, Sci. Rep. 5 (2015) 13698.
[76] M. Wuttig, V.L. Deringer, X. Gonze, C. Bichara, J.-Y. Raty, Incipient metals: functional materials with a unique bonding mechanism, Adv. Mater. 30 (2018) 1803777.
[77] M. Wuttig, C.-F. Schön, J. Lötfering, P. Golub, C. Gatti, J.-Y. Raty, Revisiting the nature of chemical bonding in chalcogenides to explain and design their properties, Adv. Mater. 35 (2023) 2208485.
[78] B. Huang, J. Robertson, Bonding origin of optical contrast in phase-change memory materials, Phys. Rev. B 81 (2010) 081204.
[79] R.O. Jones, S.R. Elliott, R. Dronskowski, The myth of "metavalency" in phase-change materials, Adv. Mater. 35 (2023) 2300836.
[80] M. Wuttig, C.-F. Schön, D. Kim, P. Golub, C. Gatti, J.-Y. Raty, B.J. Kooi, A. Martín Pendás, R. Arora, U. Waghmare, Metavalent or hypervalent bonding: is there a chance for reconciliation? Adv. Sci. 11 (2024) 2308578.
[81] K. Ruedenberg, The physical nature of the chemical bond, Rev. Mod. Phys. 34 (1962) 326–376.

Robert O. Jones studied Physics and Mathematics at the University of Western Australia in Perth and obtained his Ph.D. from the University of Cambridge under Volker Heine on surface states in semiconductors. He spent three years as postdoctoral associate at Cornell University before joining the Forschungszentrum Jülich. His main focus for over 40 years has been on density functional theory and its applications to ordered and disordered systems [solids, surfaces, atomic clusters, molecules (including biological molecules), polymers, glasses, etc.], most recently on the theory of the chemical bond.